

NO-A198 492

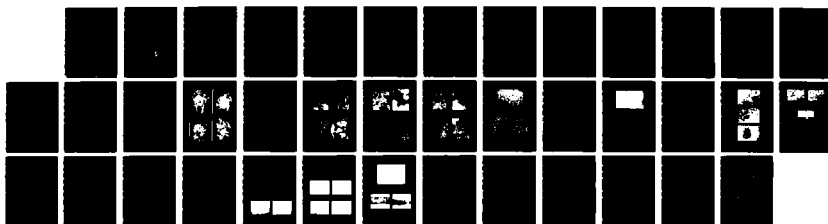
GROWTH AND DEFORMATION MECHANISMS OF REFRACTORY ALLOY  
HYBRID MATERIALS. (U) MCDONNELL DOUGLAS RESEARCH LABS  
ST LOUIS MO S H SASTRY ET AL DEC 87 NDC-08082  
AFOSR-TR-87-2848 F49620-86-C-0108

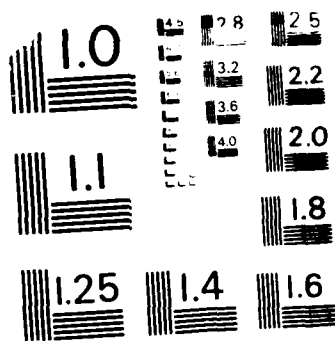
1/1

UNCLASSIFIED

F/G 11/6.1

NL





MICROCOPY RESOLUTION TEST CHART  
NATIONAL BUREAU OF STANDARDS - 1963-A

2

DTIC FILE COPY

AFOSR-TR. 87-2040

MDC Report No. QA002

AD-A190 492

# GROWTH AND DEFORMATION MECHANISMS OF REFRACTORY ALLOY HYBRID MATERIALS

S. M. L. Sastry  
D. M. Bowden  
B. D. London  
R. J. Lederich  
J. E. O'Neal

McDonnell Douglas Research Laboratories  
St. Louis, Missouri 63166

December 1987

Annual Technical Report for the Period 15 September 1986—15 September 1987

Approved for public release; distribution unlimited

The views and conclusions contained in this document are those of the authors and should not be interpreted as necessarily representing the official policies or endorsements, either expressed or implied, of the Air Force Office of Scientific Research of the U. S. Government.

Prepared for:  
UNITED STATES AIR FORCE  
Air Force Office of Scientific Research  
Bolling Air Force Base, DC 20332

DTIC  
ELECTE  
JAN 20 1988  
S  
AD

3 014

# REPORT DOCUMENTATION PAGE

1a. REPORT SECURITY CLASSIFICATION UNCLASSIFIED			1b. RESTRICTIVE MARKINGS		
2a. SECURITY CLASSIFICATION AUTHORITY			3. DISTRIBUTION/AVAILABILITY OF REPORT Approved for public release, distribution unlimited		
2b. DECLASSIFICATION/DOWNGRADING SCHEDULE			5. MONITORING ORGANIZATION REPORT NUMBER(S) <b>AFOSR-TR- 87-2040</b>		
4. PERFORMING ORGANIZATION REPORT NUMBER(S) MDC QA002			7a. NAME OF MONITORING ORGANIZATION <i>Same as 8a</i>		
6a. NAME OF PERFORMING ORGANIZATION McDonnell Douglas Research Laboratories		6b. OFFICE SYMBOL (If applicable)	7b. ADDRESS (City, State, and ZIP Code) <i>Same as 8c</i>		
6c. ADDRESS (City, State, and ZIP Code) McDonnell Douglas Corporation P.O. Box 516 St. Louis, MO 63166		8b. OFFICE SYMBOL (If applicable)	9. PROCUREMENT INSTRUMENT IDENTIFICATION NUMBER F49620-86-C-0108		
8a. NAME OF FUNDING/SPONSORING ORGANIZATION Air Force Office of Scientific Research		10. SOURCE OF FUNDING NUMBERS			
8c. ADDRESS (City, State, and ZIP Code) Building 410 Bolling AFB, DC 20332-6448		PROGRAM ELEMENT NO. <i>61102F</i>	PROJECT NO. <i>2306</i>	TASK NO. <i>A1</i>	WORK UNIT ACCESSION NO.
11. TITLE (Include Security Classification) GROWTH AND DEFORMATION MECHANISMS OF REFRACTORY ALLOY HYBRID MATERIALS					
12. PERSONAL AUTHOR(S) S. M. L. Sastry, D. M. Bowden, B. D. London, R. J. Lederich, J. E. O'Neal					
13a. TYPE OF REPORT Annual Technical Rpt		13b. TIME COVERED FROM 9/86 TO 9/87		14. DATE OF REPORT (Year, Month, Day) 1987 Dec 18	
15. PAGE COUNT 30					
16. SUPPLEMENTARY NOTATION					
17. COSATI CODES			18. SUBJECT TERMS (Continue on reverse if necessary and identify by block number)		
FIELD	GROUP	SUB-GROUP	titanium alloys, niobium alloys, hybrid materials, refractory materials, rapid solidification processing, oxide dispersions, in-situ composites, whisker reinforcement, mechanical		
19. ABSTRACT (Continue on reverse if necessary and identify by block number) Oxide-dispersion-strengthened and whisker/particulate reinforced titanium and niobium alloys produced by rapid solidification processing are being investigated with the objectives of understanding the mechanisms of formation and growth of the secondary phases and how these factors determine strengthening mechanisms and thermal stability of Ti and Nb alloys. During the first year of the three-year program, Ti alloys containing Al, Er, B, and C, and Nb alloys containing W, Hf, La, B, and C were prepared by nonconsumable electrode arc melting and microstructures were characterized. The alloys were rapidly solidified by electron beam melting and splat quenching and the rapidly solidified flakes were characterized by x-ray diffraction, optical metallography, and electron microscopy. The mechanical properties of rapidly solidified Ti alloys containing Er, B, and C were determined by tensile testing of specimens prepared from electron-beam-melted and splat-quenched flakes.					
20. DISTRIBUTION/AVAILABILITY OF ABSTRACT <input type="checkbox"/> UNCLASSIFIED/UNLIMITED <input checked="" type="checkbox"/> SAME AS RPT <input type="checkbox"/> DTIC USERS			21. ABSTRACT SECURITY CLASSIFICATION UNCLASSIFIED		
22a. NAME OF RESPONSIBLE INDIVIDUAL <i>[Signature]</i>			22b. TELEPHONE (Include Area Code) <i>202 767-4933</i>		22c. OFFICE SYMBOL <i>NE</i>

18. continued

properties, deformation mechanisms, growth kinetics, work hardening.

Accession For	
NTIS CRA&I	<input checked="checked" type="checkbox"/>
DTIC TAB	<input type="checkbox"/>
Unannounced	<input type="checkbox"/>
Justification	
By	
Distribution	
Availability Codes	
Dist	Avail and/or Special
A-1	



## TABLE OF CONTENTS

Section	Page
1. INTRODUCTION.....	1
2. RESEARCH OBJECTIVES AND APPROACH.....	3
3. SUMMARY OF RESULTS.....	7
3.1 Rapid Solidification Processing of Titanium Alloys.....	7
3.2 Microstructures and Properties of Titanium Alloys.....	10
3.3 Rapid Solidification Processing of Niobium Alloys.....	23
3.4 Microstructures of Niobium Alloys.....	24
4. PUBLICATIONS RESULTING FROM THIS CONTRACT.....	27
5. LIST OF PERSONNEL.....	28
6. COUPLING ACTIVITIES WITH GROUPS DOING RELATED RESEARCH.....	29
7. REFERENCES.....	30

# LIST OF ILLUSTRATIONS

Figure	Page
1. Flow diagram of Phase I.....	4
2. Flow diagram of Phase II.....	5
3. Flow diagram of Phase III.....	6
4. Schematic diagram of the electron-beam melting/splat-quenching apparatus for the rapid solidification of titanium.....	8
5. Rapidly solidified flakes of (a) Ti-1.25 Er, (b) Ti-1.5B, (c) Ti-36Al-2Er, and (d) Ti-36Al-1.5B alloys produced by electron-beam melting/splat quenching.....	9
6. As-cast microstructures of (a) Ti-2Er and (b) Ti-4Er alloys.....	11
7. As-cast microstructures of (a) Ti <sub>3</sub> Al-2Er and (b) Ti <sub>3</sub> Al-4Er alloys.....	11
8. As-cast microstructures of (a) TiAl-2Er and (b) TiAl-4Er alloys..	12
9. As-cast microstructures of (a) Ti-1.5B and (b) Ti-3B alloys.....	12
10. As-cast microstructures of (a) Ti <sub>3</sub> Al-1.5B and (b) Ti <sub>3</sub> Al-3B alloys.....	13
11. As-cast microstructures of (a) TiAl-1.5B and (b) TiAl-3B alloys..	13
12. As-cast microstructure of Ti-1.0C alloy.....	14
13. As-cast microstructures of (a) Ti <sub>3</sub> Al-1C and (b) Ti <sub>3</sub> Al-2C alloys..	14
14. Microstructure of rapidly solidified Ti-2Er alloy.....	16
15. Microstructures of Ti-1.0B; (a) as-rapidly solidified, (b) annealed at 800°C/2 h, and (c) annealed at 900°C/1 h.....	18
16. Microstructure of Ti-1.0C alloy (a) as-rapidly solidified and (b) annealed at 840°C/2 h.....	19
17. Tensile specimen machined from electron-beam-melted/splat-quenched flakes of Ti alloys.....	19
18. Grip assembly for gripping thin tensile specimens.....	19
19. Stress-strain curves of rapidly solidified (a) Ti, (b) Ti-2Er, (c) Ti-0.5B, and (d) Ti-1.0C alloys.....	20
20. Stress-strain curves of rapidly solidified Ti-0.5B annealed at (a) 700°C/2 h, (b) 810°C/4h, (c) 800°C/18 h, and (d) 900°C/2 h...	21

**LIST OF ILLUSTRATIONS**  
(continued)

<b>Figure</b>	<b>Page</b>
21. Comparisons of stress-strain curves of Ti and Ti-0.5B alloy.....	22
22. As-cast microstructures of (a) Nb-2Al and (b) Nb-15Hf-2La alloys.	24
23. As-cast microstructures of (a) Nb-15W-2La and (b) Nb-30W-2La alloys.....	25
24. As-cast microstructures of (a) Nb-1Y and (b) Nb-15W-1Y alloys....	25
25. As-cast microstructures of Nb-0.2C alloy.....	26
26. Microstructures of electron-beam-melted/splat-quenched flakes of (a) Nb-2La and (b)Nb-15Hf-1Y alloys.....	26

## LIST OF TABLES

Table		Page
1.	Nominal Compositions of Titanium Alloys.....	7
2.	Summary of X-ray Diffraction Results From Electron-Beam-Melted/ Splat-Quenched Ti Alloy Flakes.....	15
3.	Nominal Compositions of Niobium Alloys.....	23

## 1. INTRODUCTION

Rapid solidification technology (RST) applied to titanium and niobium alloys can produce oxide-dispersion-strengthened alloys, which have large volume fractions of  $< 0.1\text{-}\mu\text{m}$  incoherent oxide dispersoids, and *in situ* composites containing high-modulus whisker/particulate reinforcements (References 1-10). The alloys so produced are a special class of refractory hybrid materials which are light weight and have the high-temperature strength and stability required for hypersonic aircraft skins and structures.

Oxide dispersions in RST titanium alloys are produced by rapid solidification processing and subsequent annealing of Ti/rare-earth (rare earth = Ce, Dy, Er, Gd, La, Nd, or Y) alloys. Rapid solidification significantly increases the solid solubilities of rare-earth elements in Ti; subsequent annealing results in scavenging by rare-earth elements of interstitial oxygen from the Ti matrix and formation of rare-earth oxide dispersoids.

RST *in situ* composites are so named because they contain large volume fractions of reinforcing second-phase particles reminiscent of the filaments or whiskers used in metal-matrix composites. These reinforcing dispersoids are formed *in situ* in RST alloys either upon solidification or subsequently by the controlled decomposition of the supersaturated solid solutions achievable only by RST. The physical conditions that govern the nucleation, growth, and matrix interactions of the reinforcing dispersoids in RST *in situ* composites are different from those that prevail in conventional alloys or metal matrix-composites.

The basic mechanisms by which oxide-dispersion-strengthened alloys and *in situ* composites are formed and by which are imparted with stable high-temperature strength are not known quantitatively. The objective of the present investigation is to develop predictive models to describe the morphology and growth kinetics of the reinforcement phases and mechanical behavior of novel hybrid materials produced by rapid solidification processing (RSP). Ti and Nb alloys containing large-aspect-ratio filamentary or spherical equiaxed boride, carbide, and oxide reinforcements are being studied to determine the mechanisms of formation and growth of the secondary phases and how these factors determine strengthening mechanisms and thermal stability of Ti and Nb alloys.

## 2. RESEARCH OBJECTIVES AND APPROACH

The objectives of the research program are to (1) develop predictive models for the formation and growth of filamentary and spherical reinforcements in RST **in situ** composites, (2) determine quantitative dependence of strength and modulus on reinforcement and matrix characteristics, and (3) perform experimental validation of the theoretical models.

The program is being performed in three phases as outlined in Figures 1-3. Phase I concentrates on the mechanisms of formation and growth kinetics of RST **in situ** composite reinforcement phases. The principal goal of Phase II is determination of the **in situ** composite strength and modulus dependencies on reinforcement and matrix parameters. The results under Phases I and II will be unified in Phase III into a comprehensive quantitative model of RST **in situ** composites. Titanium and niobium are selected as the base metals because in addition to being prime candidates for hypersonic aircraft and missiles, they also exhibit a diversity of reinforcement morphologies, characteristics, and interactions that are generally representative of RST **in situ** composites.

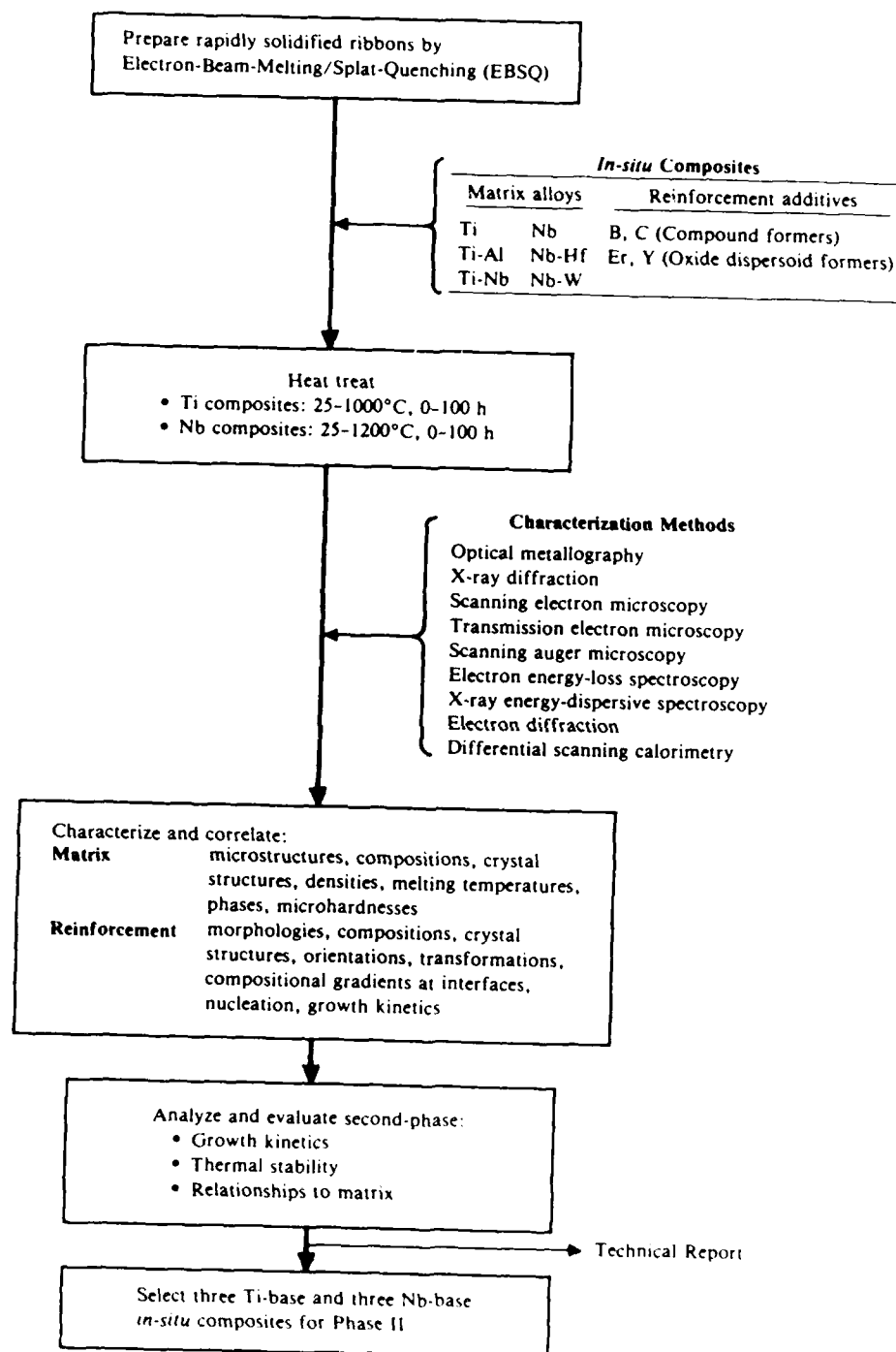


Figure 1. Flow diagram of Phase I.

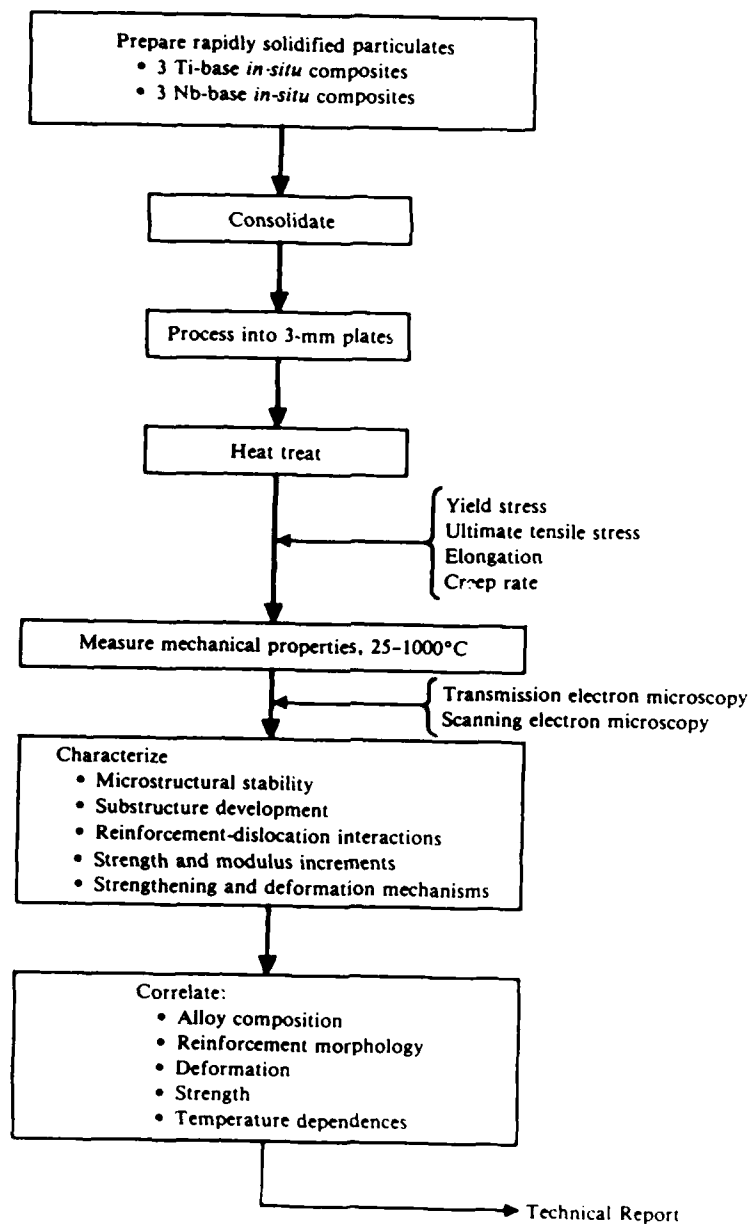
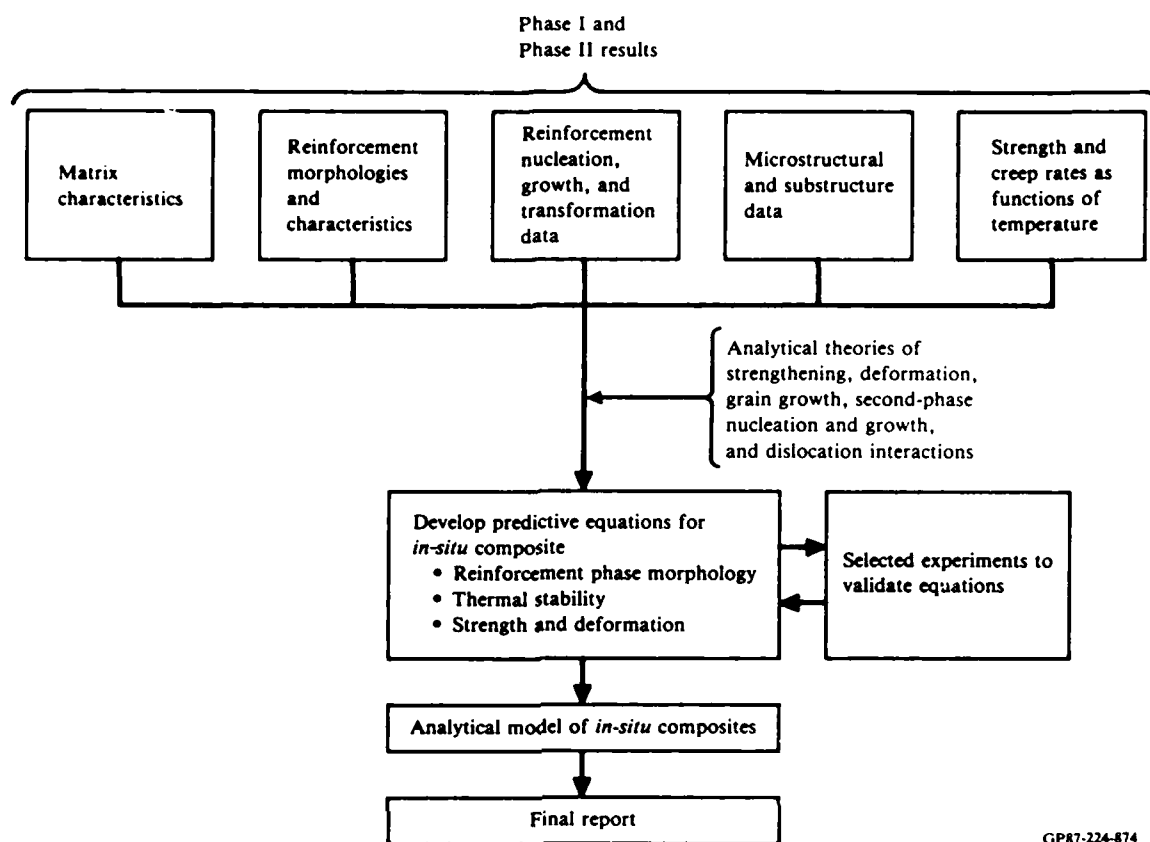


Figure 2. Flow diagram of Phase II.



**Figure 3. Flow diagram of Phase III.**

The specific objectives of Phase I of the program were as follows:

- (1) produce rapidly solidified Ti and Nb alloy particulates by electron beam melting and splat quenching of prealloyed Ti-B, Ti-C, Ti-Al-B, Ti-Al-C, Ti-Er, and Ti-Al-Er, Nb-B, Nb-C, Nb-La, Nb-Y, Nb-Hf-La, Nb-W-La, Nb-Hf-Y, Nb-Zr-C, and Nb-W-Zr-C alloys; (2) determine compositions and crystal structures of reinforcement phases and orientation relationships between matrix and reinforcement phases; (3) determine the temperature dependence of growth kinetics of reinforcement phases; and (4) select three titanium alloys and three niobium alloys containing the most stable boride, carbide, and oxide reinforcements.

### 3. SUMMARY OF RESULTS

#### 3.1 Rapid Solidification Processing of Titanium Alloys

Titanium alloys of the compositions shown in Table 1 were procured from Titanium Metals Corporation of America. Alloy compositions have been selected to complete a comprehensive catalog of the various possible matrix/reinforcement-phase combinations; the matrices cover alpha, alpha 2 ( $Ti_3Al$ ), and gamma ( $TiAl$ ) - the most important matrices in the Ti-Al system, and the reinforcements include spherical and filamentary morphologies. The erbium additions produce spherical, submicroscopic, incoherent dispersoids; the Ti-B phase forms large aspect-ratio filamentary reinforcements; the Ti-C phase is spherical.

Table 1. Nominal compositions of titanium alloys.

Alloy Number	TIMET Button Number	Nominal Composition	Matrix
1	B 8842	Ti-2Er	αTi
2	B 8849	Ti-4Er	
3	B 8859	Ti-1.5B	
4	B 8864	Ti-3.0B	
5		Ti-1.0C	
6	B 9244	Ti-16Al-2Er	α <sub>2</sub> (Ti <sub>3</sub> Al)
7	B 9245	Ti-16Al-4Er	
8	B 9246	Ti-16Al-1.5B	
9	B 9247	Ti-16Al-3.0B	
10	B 9248	Ti-16Al-1C	
11	B 9249	Ti-16Al-2C	γ (TiAl)
12	B 8914	Ti-36Al-2Er	
13	B 8922	Ti-36Al-4Er	
14	B 8930	Ti-36Al-1.5B	
15	B 8936	Ti-36Al-3.0B	

87-224-875

The alloys were prepared by nonconsumable electrode arc-melting in an argon atmosphere. Six-mm diameter, 100-mm-long rods prepared by electric discharge machining were used as feed stock for rapid solidification processing by electron-beam-melting/splat-quenching. The experimental arrangement used for electron-beam-melting/splat-quenching is shown in Figure 4. An electron beam is focused onto the end of a rotating Ti-alloy rod where it melts the surface and produces molten drops. The molten drops fall onto a rotating copper disk and are stretched into thin flakes under the combined actions of a high angular velocity and the centrifugal force of the rotating disk. Melt drop size and drip rate are controlled by varying the rotational speed of the alloy rod, vertical traverse rate of the rod, and power input to the alloy rod; flake thickness is controlled by varying the speed of the rotating copper disk. Typical flakes produced by this technique are shown in Figures 5a-5d.

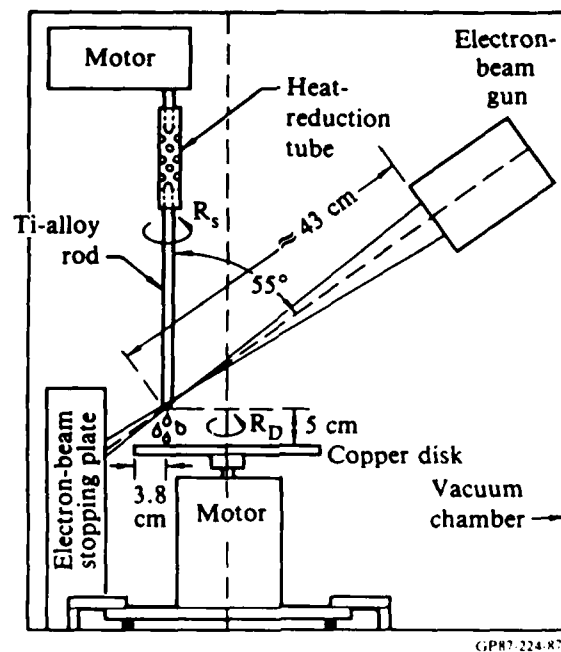


Figure 4. Schematic diagram of the electron-beam splat-quenching apparatus for the rapid solidification of titanium.

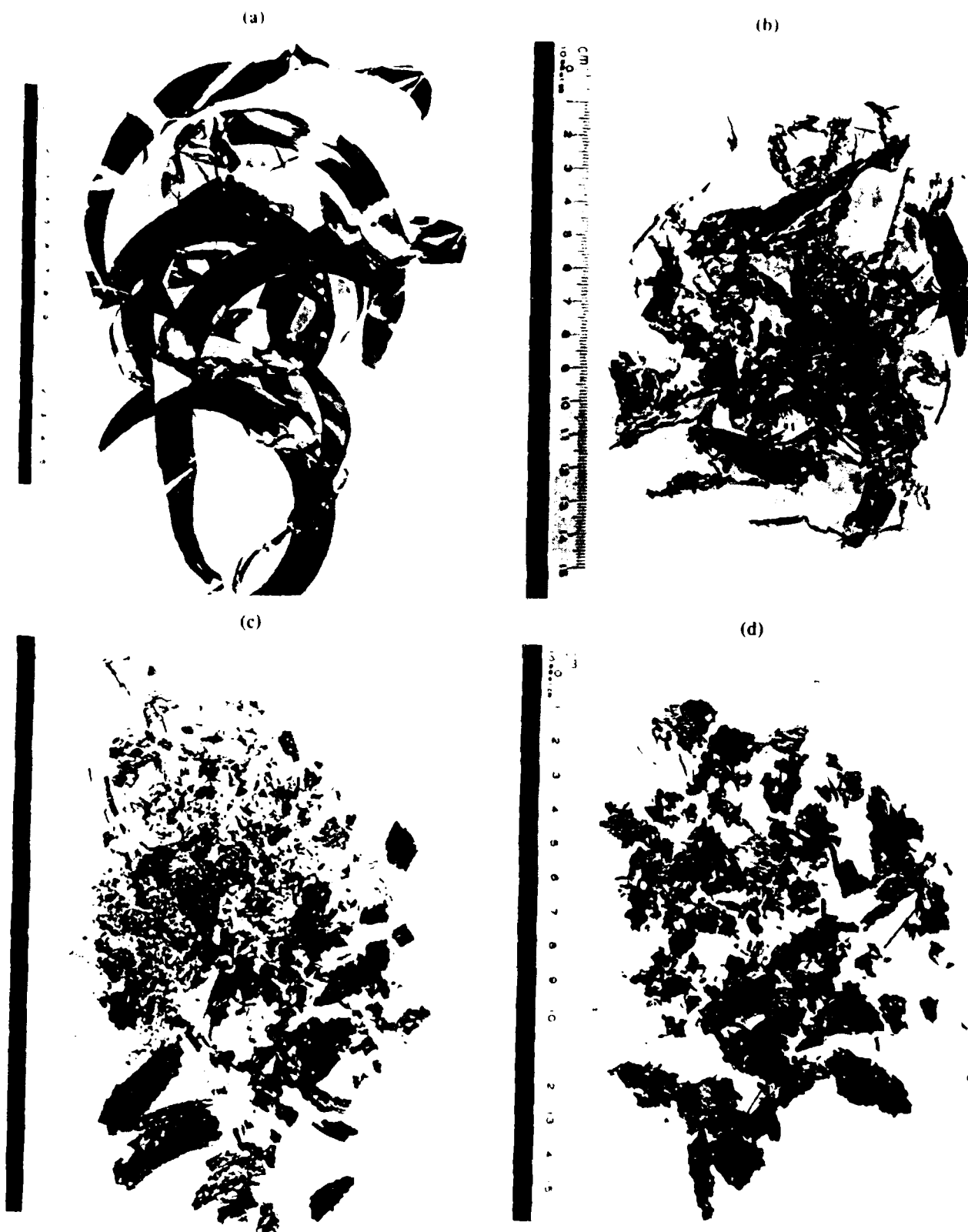


Figure 5. Rapidly solidified flakes of (a) Ti-2.0Er, (b) Ti-1.B, (c) Ti-36Al-2Er, and (d) Ti-36Al-1.5B alloys produced by electron beam melting and splat quenching.

The splat-quenching method used in the present study produces large undercoolings and high cooling rates. Perepezko and co-workers (Reference 11) have discussed the direct correlation between the extent of undercooling and the degree of compositional and microstructural refinement (viz., supersaturated solid solutions, metastable phase formation, and microcrystalline structures) produced by rapid solidification. Undercoolings of about one-third the melting point are common in the splat-quenching methods. Following nucleation, after substantial undercooling, a solidifying interface rejects latent heat both into the supercooled liquid and into the newly formed solid. The cooling rates of the splat-quenched flakes were estimated from the flake thickness by heat-transfer analysis (Reference 12). The average cooling rate as a function of splat thickness for titanium alloys was determined to be  $1.5 \times 10^5$  to  $5 \times 10^6$  K/s for flake thicknesses of 50 to 100  $\mu\text{m}$ .

The rapidly solidified flakes were sealed in quartz capsules under a vacuum of  $10^3$  Pa ( $7.5 \times 10^{-6}$  Torr), and the sealed capsules were annealed at 700, 800, and 900°C for 0.5-100 h. The rapidly solidified and annealed flakes were examined by scanning and transmission electron microscopy.

### 3.2 Microstructures and Properties of Titanium Alloys

The microstructures of arc-melted buttons of titanium based alloys are shown in Figures 6-13. Er-containing alloys contain coarse Er-rich particles precipitated mainly along prior-beta grain boundaries. The boride phase in alpha Ti and  $\text{Ti}_3\text{Al}$  has a rod-like morphology. However, in  $\text{TiAl}$ , the borides precipitate in the form of equiaxed particles. The carbide particles are spherical in all three matrices.

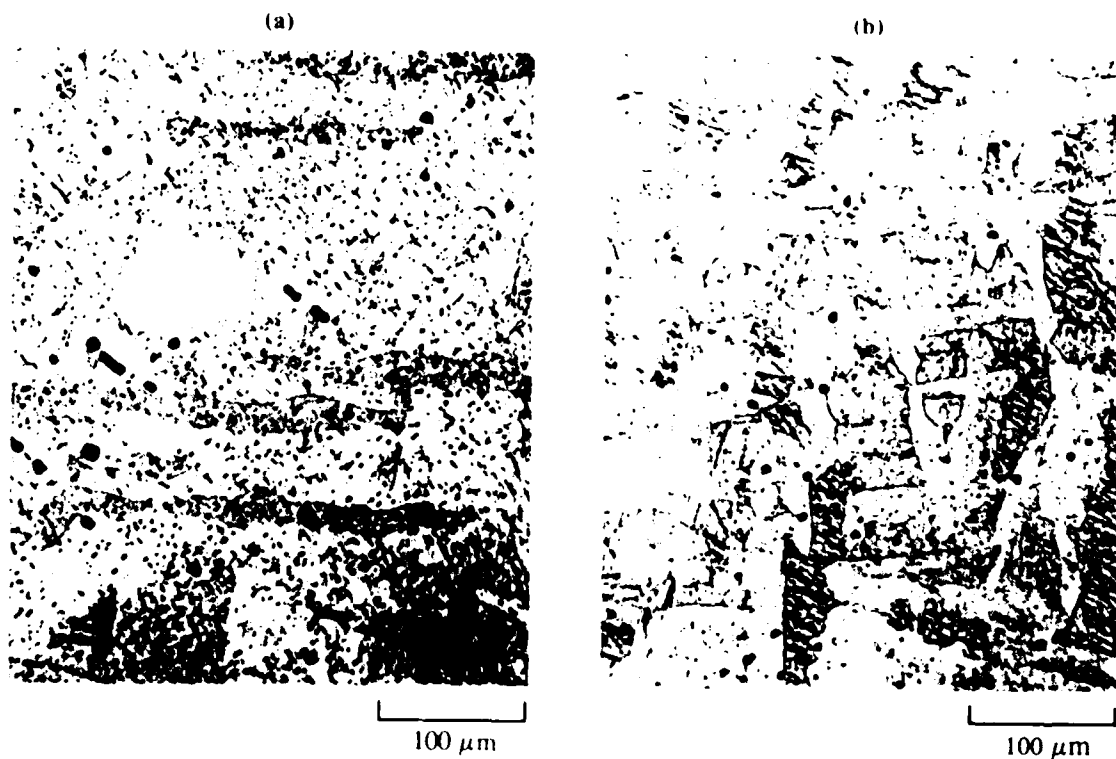


Figure 6. As-cast microstructures of (a) Ti-2Er, and (b) Ti-4Er alloys.

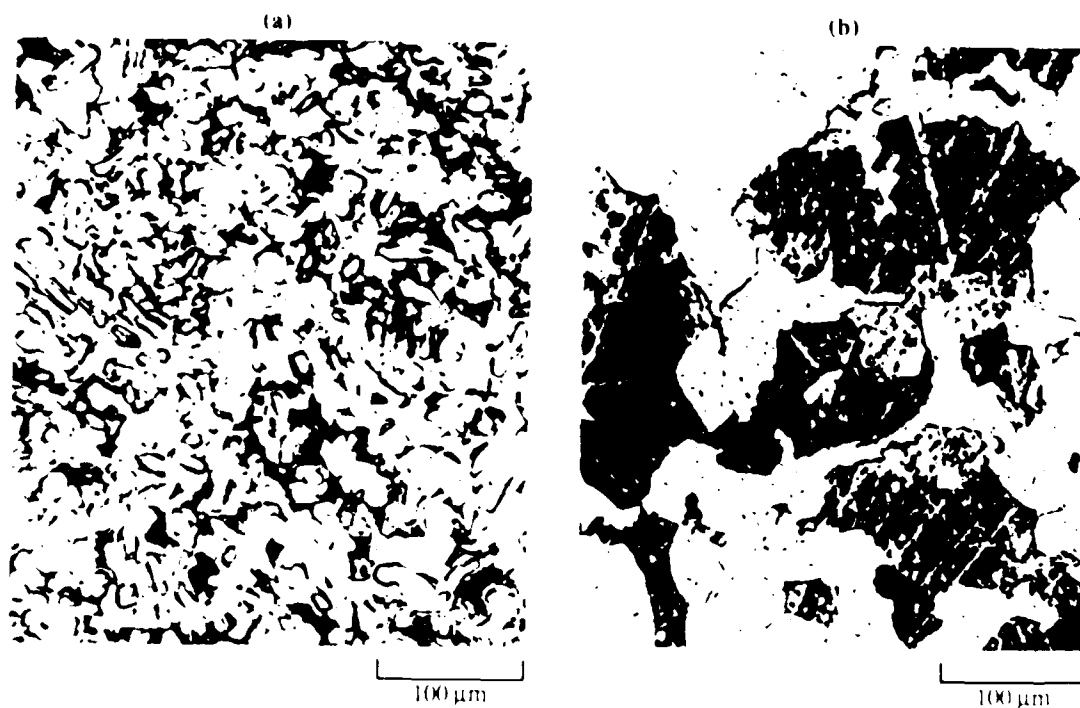


Figure 7. As-cast microstructures of (a) Ti<sub>3</sub>Al-2Er and (b) Ti<sub>3</sub>Al-4Er alloys.

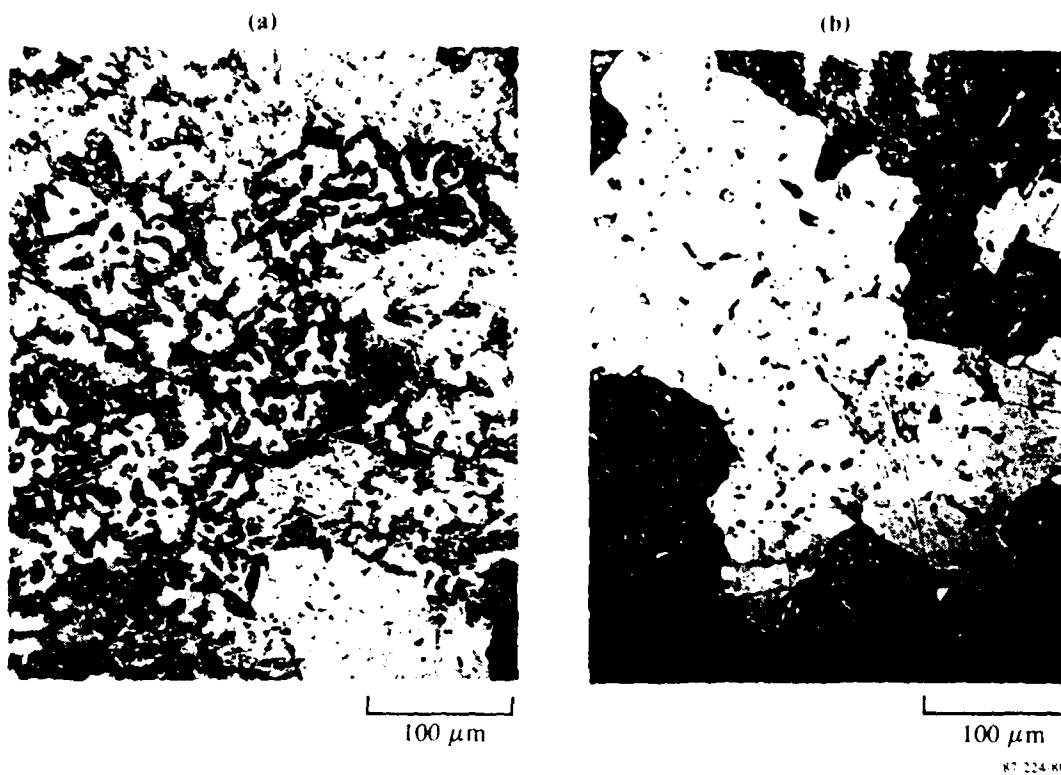


Figure 8. As-cast microstructures of (a) TiAl-2Er and (b) TiAl-4Er alloys.

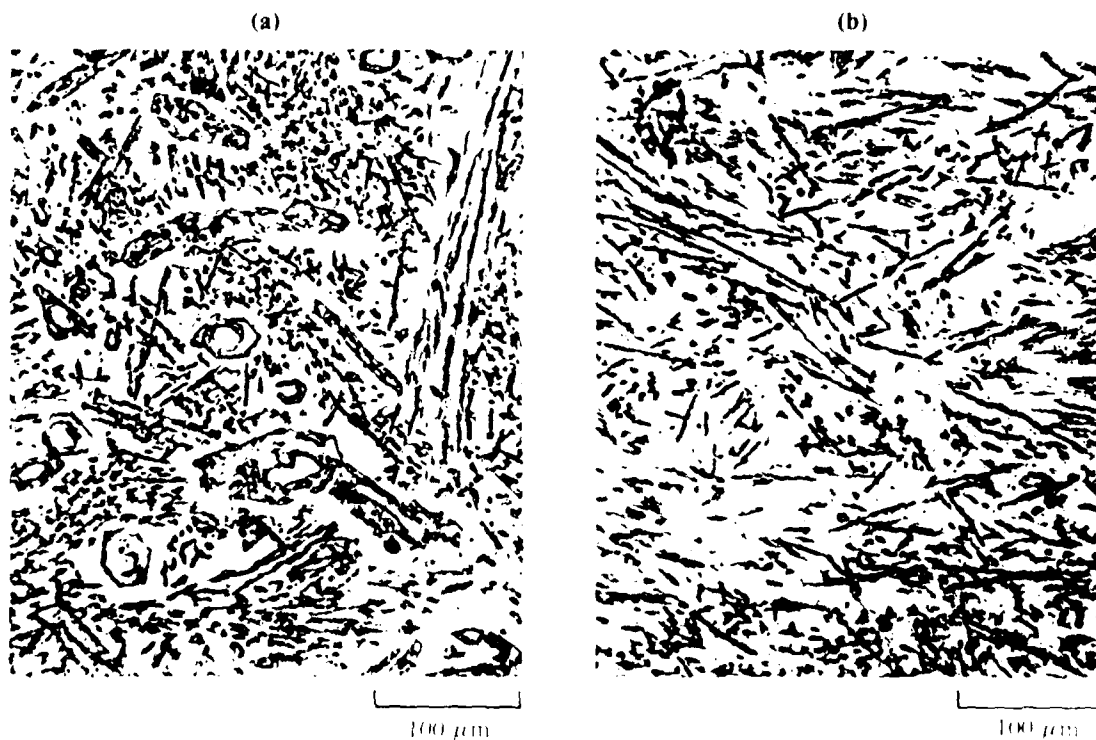


Figure 9. As-cast microstructures of (a) Ti-1.5B and (b) Ti-3B alloys.

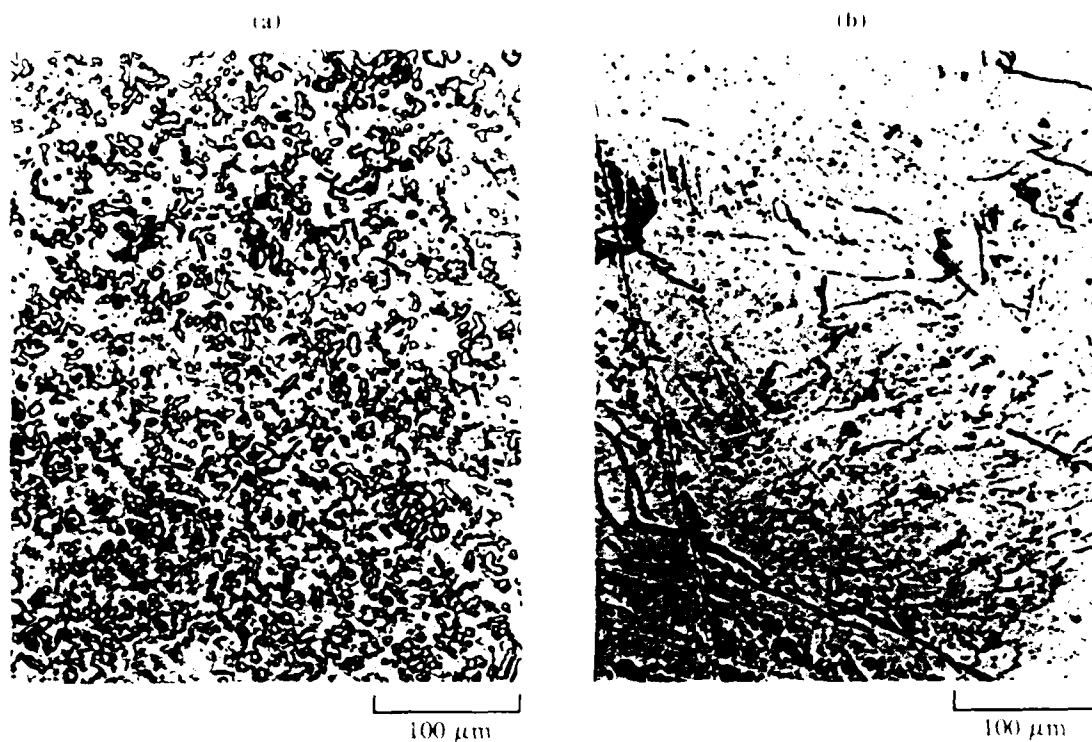


Figure 10. As-cast microstructures of (a) Ti<sub>3</sub>Al-1.5B and (b) Ti<sub>3</sub>Al-3B alloys.

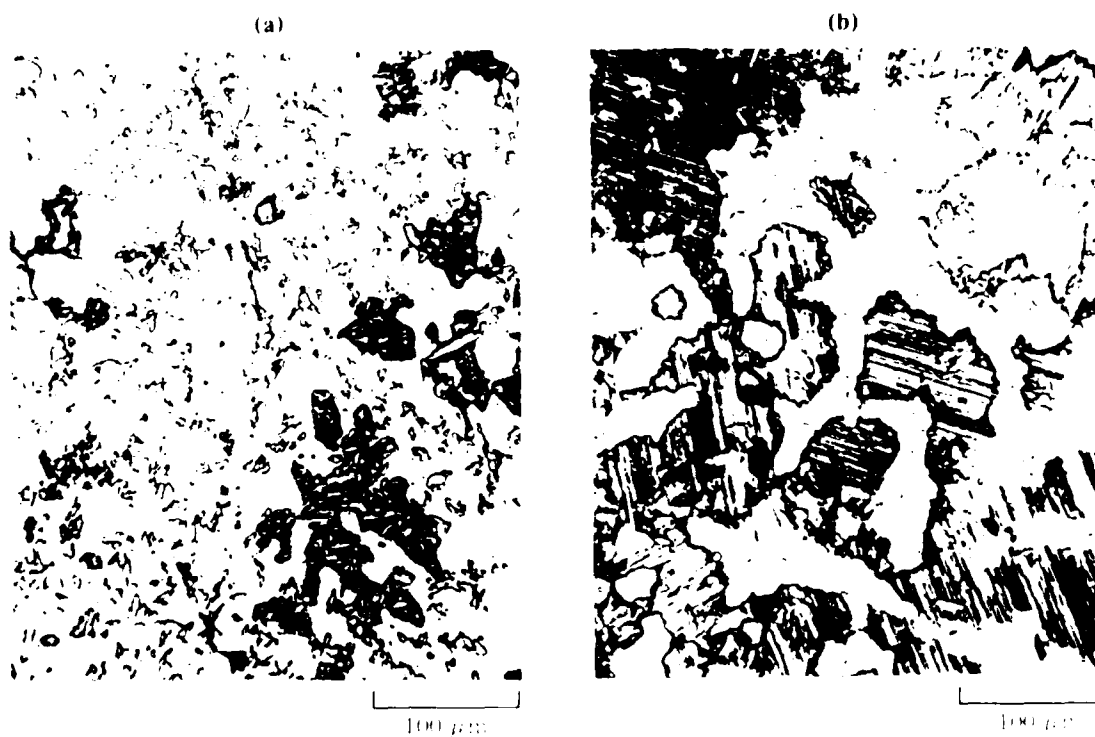


Figure 11. As-cast microstructures of (a) TiAl-1.5B and (b) TiAl-3B alloys.

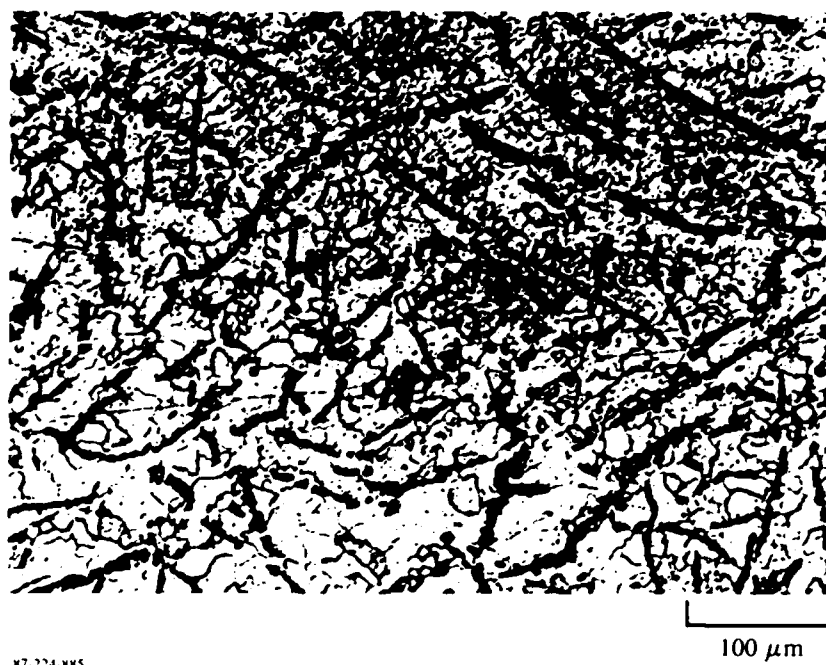


Figure 12. As-cast microstructure of Ti-1.0C alloy.

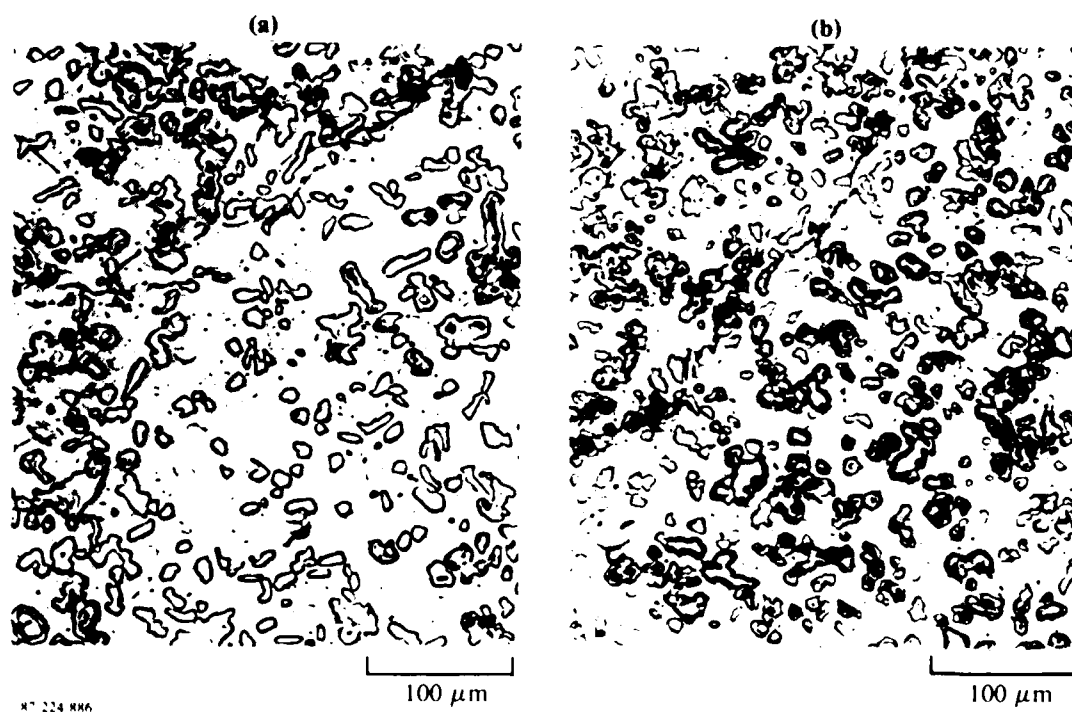


Figure 13. As-cast microstructures of (a) Ti<sub>7</sub>Al-1C and (b) Ti<sub>7</sub>Al-2C alloys.

Rapidly solidified particulates of Ti-2.0Er, Ti-1.5B, Ti-36Al-2Er, and Ti-36Al-1.5B were analyzed by x-ray diffraction for the phases present; the results are summarized in Table 2.

**Table 2. Summary of x-ray diffraction results from electron-beam melted/splat-quenched Ti alloy flakes.**

Alloy	Composition	Side	Results
1	Ti-1.25Er	B	$\alpha$ -Ti, No evidence of Er or $\text{Er}_2\text{O}_3$ , some small unidentified peaks
		A	Same as side B
3	Ti-1.5B	B	$\alpha$ -Ti, some small evidence of TiB (one small peak)
		A	Same as side B
5	Ti-36Al-2Er	B	Mostly TiAl ( $\gamma$ ), small amount of $\text{Ti}_3\text{Al}$ ( $\alpha_2$ )
		A	Mostly TiAl ( $\alpha$ ), more $\text{Ti}_3\text{Al}$ ( $\alpha_2$ ) than in side B
7	Ti-36Al-1.5B	B	Mostly TiAl ( $\gamma$ ), small amount of $\text{Ti}_3\text{Al}$ ( $\alpha_2$ )
			Mostly TiAl ( $\gamma$ ), more $\text{Ti}_3\text{Al}$ ( $\alpha_2$ ) than side B, evidence of $\text{TiB}_2$

87-224-876

Figure 14 shows the microstructures of RST Ti-2.0Er alloy. Whereas the microstructures of the I/M alloys consist of coarse, equilibrium Er-rich particles, RST results in a redissolution of coarse particles and homogeneous precipitation of fine 100- to 200-nm-diameter dispersoids. Free-energy considerations in the liquid state of Ti-RE-O system favor the dissolution of rare-earth oxides in the titanium melt because of the large solubilities of oxygen in the molten titanium. The phase diagram of the Ti-Er system predicts that elemental rare-earth dispersoids should form upon cooling from the melt, provided that the solid solubility limit is not exceeded. Because of the presence of 0.1 wt% oxygen in the alloy investigated, and because of the high affinity of Er for oxygen, one would expect that the oxygen dissolved in the alloys would be scavenged by the rare earths to form rare-earth oxide dispersoids. The extent to which this oxidation occurs has been evaluated by

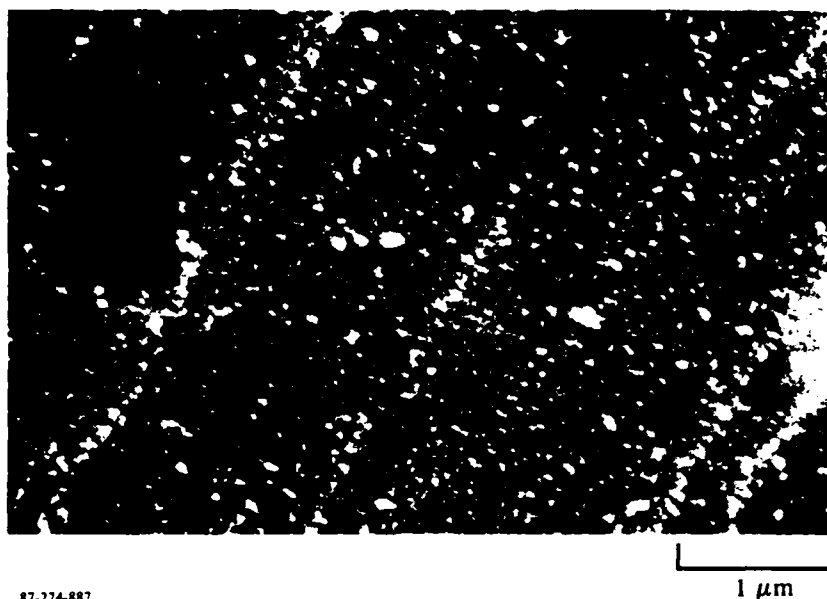


**Figure 14. Microstructure of rapidly solidified Ti-2Er alloy.**

calculating the Ti-rich corner of the Ti-Er-O systems based on the thermodynamic properties and phase diagrams of the binary Ti-Re, Ti-O, and RE-O systems. The calculated phase diagrams indicate that most of the rare earths added to Ti should be present as oxides at thermodynamic equilibrium. The I/M alloys solidify essentially under equilibrium conditions, and therefore, the particles are definitely rare-earth oxide particles. The RSP alloys, however, show extended, metastable, solid solubility of rare earths and solidification in these alloys occurs under nonequilibrium conditions. Because of the high cooling rates, the dispersoids are significantly smaller in the RSP alloys. Annealing the RSP Ti-Er alloys at temperatures below the beta transus results in coarsening of the dispersoids. The coarsening of dispersoids is related to the solubility product  $C_0 D$  where  $C_0$  is the solubility and  $D$  is the diffusivity of the rate-controlling diffusing species.

The phase diagram of Ti-B shows restricted solubility of B in both alpha- and beta-Ti (Reference 13), but large solubility increments can be obtained by rapid solidification. The Ti-1 wt% (4.3 at. %) B alloy forms fine martensite upon electron-beam melting and splat quenching (Figure 15a). Annealing the splat-quenched flakes at 700-900°C recrystallizes alpha' to alpha and produces distributions of dispersoids tentatively identified as TiB (Figures 15b and 15c). The extended solid solubility of B in Ti is in excess of the equilibrium solid solubility, and the thermal stability of the fine dispersoids is exceptional.

The phase diagram of Ti-C shows somewhat greater solubility for C in alpha-Ti than for B (Reference 14). The slope of the solidus in this system is rather shallow, so that large degrees of supersaturation are possible, provided that the precipitation of TiC can be suppressed. Because the beta-to-alpha transformation is peritectoid, supersaturated alpha solid solutions cannot be achieved by conventional means. Rapid solidification of Ti-C alloys refines the grain structure and greatly increases the amount of C in solid solution. The latter effect is due to the favorable slope of the metastable solidus extension. Upon heat treatment of the extended solid solutions, nonstoichiometric  $\text{TiC}_x$  ( $x = 0.5-0.6$ ) is formed (Figures 16a and 16b).

A tensile specimen (Figure 17) and a grip assembly (Figure 18) were used for tensile testing of small tensile specimens machined directly from electron-beam-melted and splat-quenched Ti alloy flakes.

The stress-strain curves of rapidly solidified Ti, Ti-2Er, Ti-0.5B, and Ti-1.0C alloys in the rapidly solidified and differently heat-treated conditions are shown in Figures 19 and 20. The yield stresses and work-hardening rates are significantly higher in Ti alloys containing Er, B, and C than in unalloyed Ti.

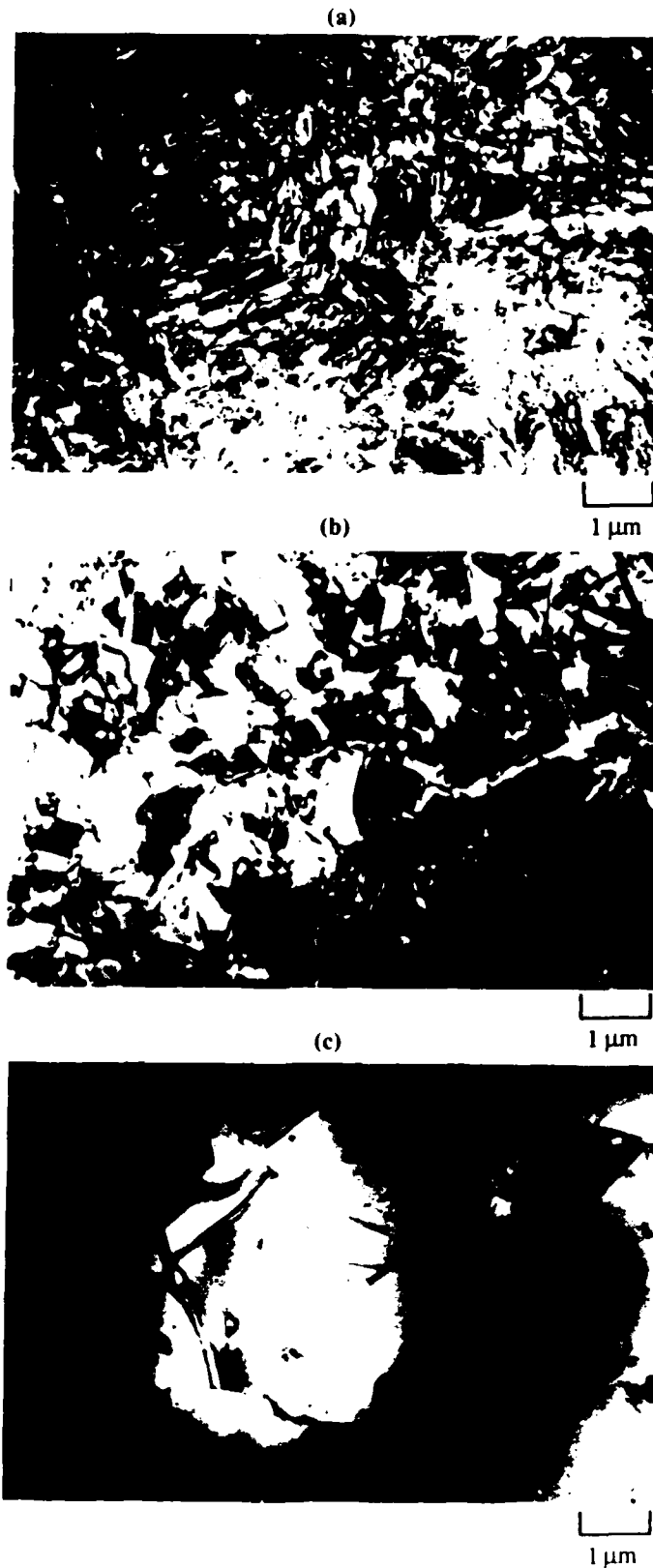


Figure 15. Microstructures of Ti-1.0B alloy; (a) as-rapidly solidified, (b) annealed at 800°C/2 h, and (c) annealed at 900°C/1 h.

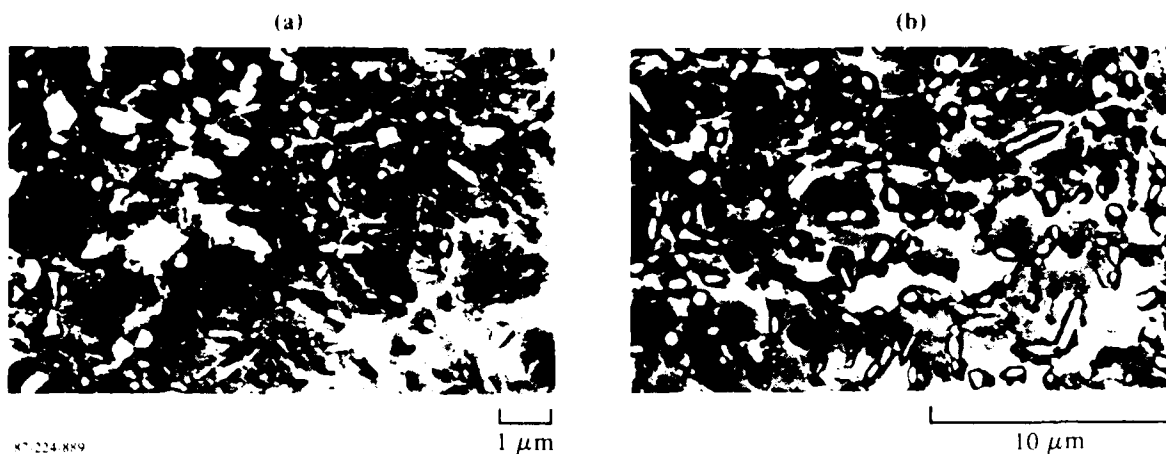


Figure 16. Microstructures of Ti-1.0C alloy (a) as rapidly solidified and (b) annealed at 840°C/2 h.

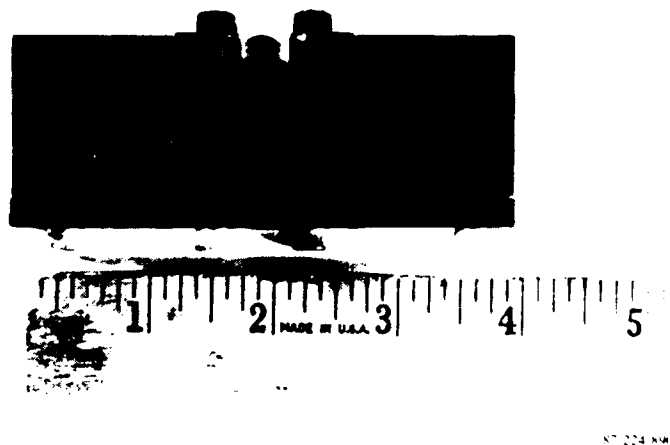
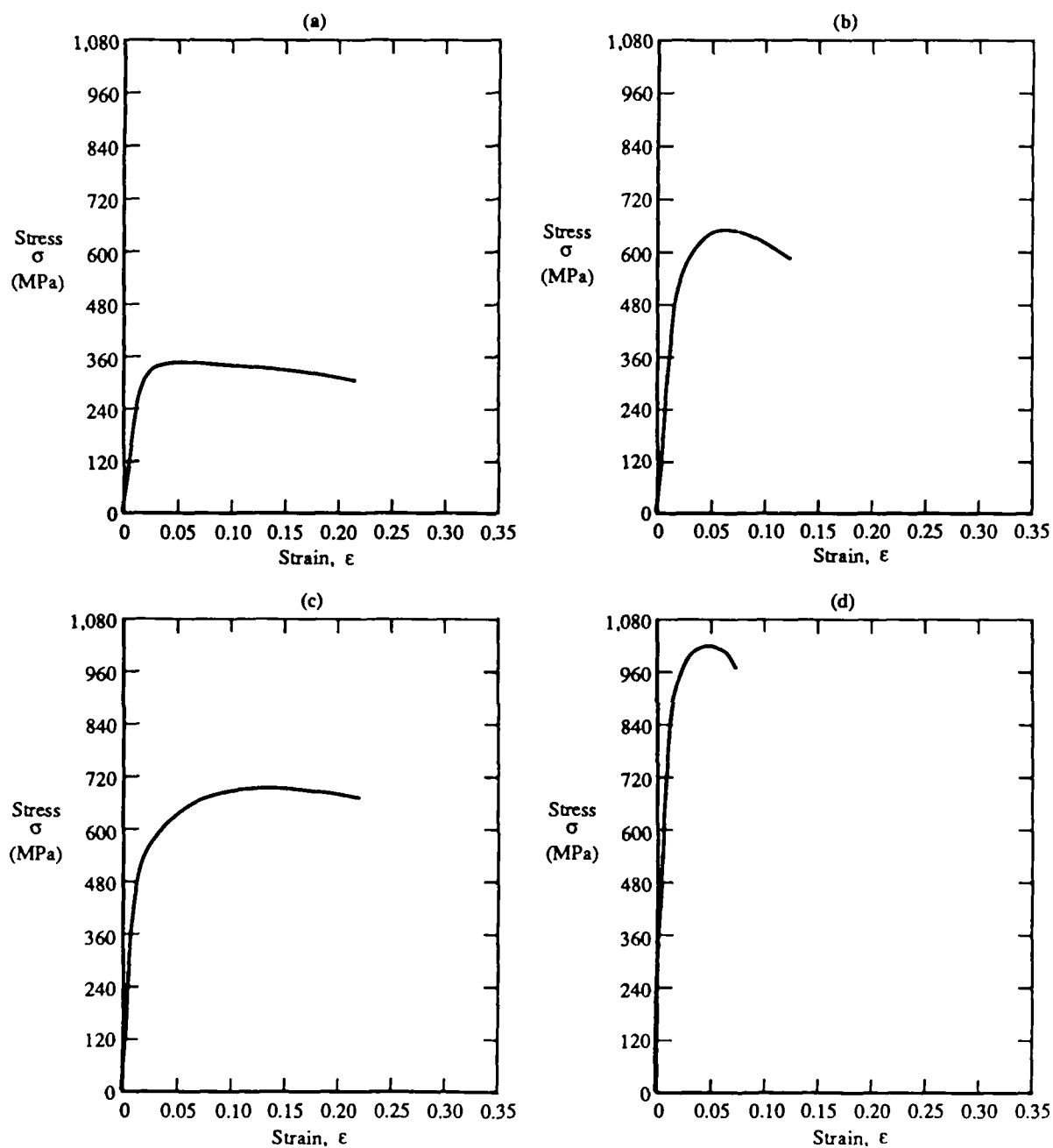


Figure 17. Grip assembly for gripping thin tensile specimens.



Figure 18. Tensile specimen machined from electron beam melted/splat quenched flakes of Ti alloy.



87-224-892.D

Figure 19. Stress-strain curves of rapidly solidified (a) Ti, (b) Ti-2Er, (c) Ti-0.5B, and (d) Ti-1.0C alloys.

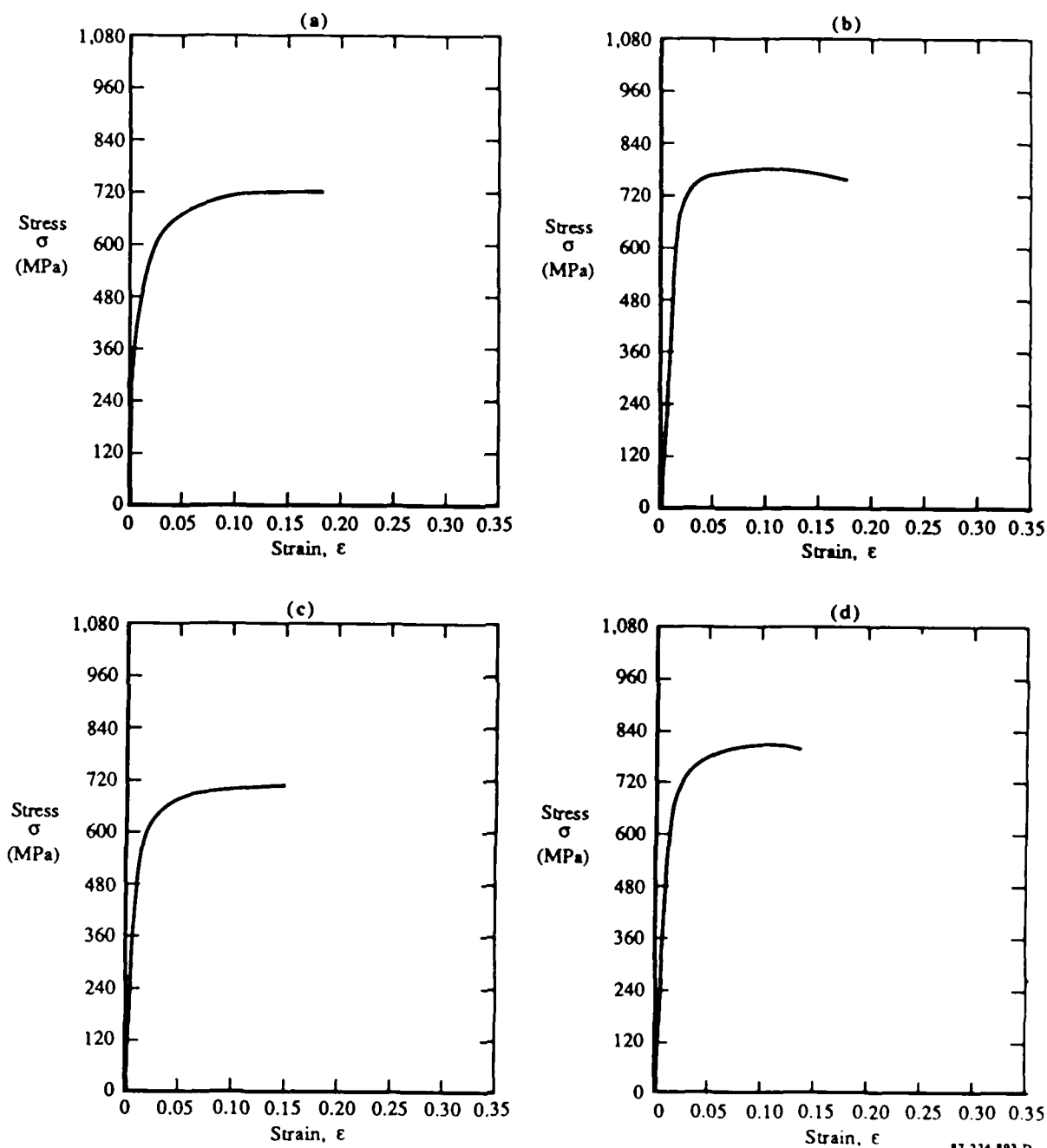


Figure 20. Stress-strain curves of rapidly solidified Ti-0.5B annealed at (a) 700°C/2 h, (b) 810°C/4 h, (c) 800°C/18 h, and (d) 900°C/2 h.

The tetrahedrally coordinated radius of B is 0.088 nm (Reference 15) which lies between the radii of the Ti atom (0.145 nm) and the largest available interstitial position (0.043 nm). Regardless of whether B is substitutionally or interstitially dissolved, the degree of distortion of the lattice and solution strengthening per wt% are expected to be high. Figure 21 is a comparison of stress-strain characteristics of Ti-B alloys and unalloyed Ti.

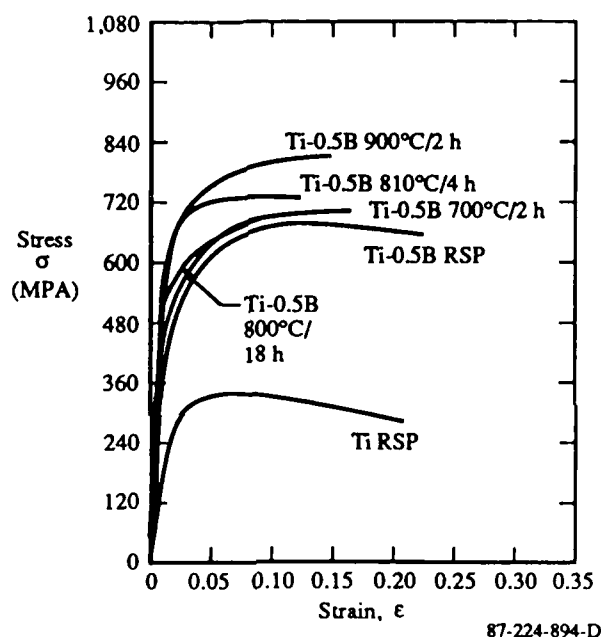


Figure 21. Comparison of stress-strain curves of Ti and Ti-0.5B alloys.

Ti-1C alloy has very high yield stress in the as-rapidly-solidified condition. Since the carbon atom has a radius of about 0.07 nm, it is probably dissolved interstitially in titanium. Carbon is expected to be a strong solid-solution strengthener because the carbon atom is considerably larger than the tetrahedral interstitial position in beta-Ti (0.043 nm) (Reference 16).

### 3.3 Rapid Solidification Processing of Niobium Alloys

Niobium alloys of compositions listed in Table 3 were procured from Teledyne Wah Chang, Albany, Oregon. Initial attempts to produce Nb-Er alloys were unsuccessful due to volatilization of the Er during melting. The rare earths Y and La were selected because of their high heats of vaporization, and ingots containing these elements were successfully produced. The La- and Y-containing alloys will allow us to study growth of rare-earth dispersoids in various niobium solid-solution matrices. Since both W and Hf are common solid-solution-strengthening additions in commercial niobium alloys, they are valid choices for solute addition. Furthermore, W and Hf provide different levels of matrix lattice strain and influence diffusion (and thus growth kinetics) differently. The carbon-containing alloys contain carbide platelet second phases. In the Zr-containing alloy, the relative stabilities of NbC and ZrC will be determined and the possible formation of NbC-ZrC solid solution will be assessed. In the Nb-30W-6Zr-0.2C alloy, the influence of W in solid solution on formation of the ZrC phase will be examined.

Table 3. Nominal compositions of niobium alloys.

Nb-2La
Nb-15Hf-2La
Nb-15W-2La
Nb-30Hf-2La
Nb-30W-2La
Nb-15Hf-1Y
Nb-15W-1Y
Nb-0.2C
Nb-6Zr-0.2C
Nb-30W-6Zr-0.2 C

GPR 224 877

The niobium alloys were prepared by nonconsumable electrode arc-melting and were rapidly solidified by electron-beam melting and splat quenching employing the same procedure used for titanium alloys.

### 3.4 Microstructures of Niobium Alloys

Typical as-cast microstructures are illustrated in Figures 22-25. The rare-earth-containing alloys show large, spherical, particles of rare earths and significant segregation of the rare earths. The carbon-containing alloys show coarse carbide platelets, which neutron diffraction studies have shown to be the  $\text{Nb}_2\text{C}$  phase.

Figures 26a and 26b show the cross sections of flakes produced by electron-beam melting and splat quenching. For the binary Nb-2La alloy (Figure 26a) the microstructure consists of columnar grains which have grown completely through the thickness of the ribbon. This microstructure is typical of ribbons in which partitionless solidification has occurred during the entire solidification process. For the ternary Nb-15Hf-1Y ribbon, however, a transition from the columnar partitionless-solidification structure

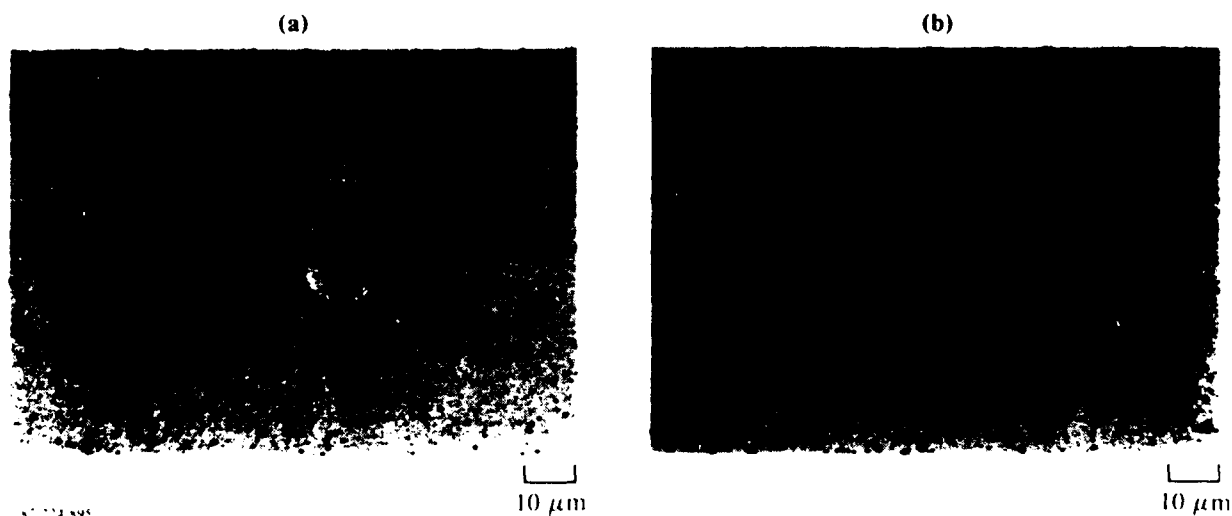


Figure 22. As-cast microstructures of (a) Nb-2La and (b) Nb-15Hf-2La alloys.

to a partitional cellular/dendritic structure is observed approximately halfway through the ribbon thickness (Figure 26b). This type of transition, typically observed in alloy ribbons, reflects the variation in cooling rate with the thickness of a ribbon. Midway through the ribbon thickness, the solidification-front velocity is not sufficiently fast for complete solute trapping, and segregation occurs. For the case of the Nb-15Hf-1Y ribbon, this segregation is probably due to coring, with the interdendritic regions becoming enriched in the solute element Hf.

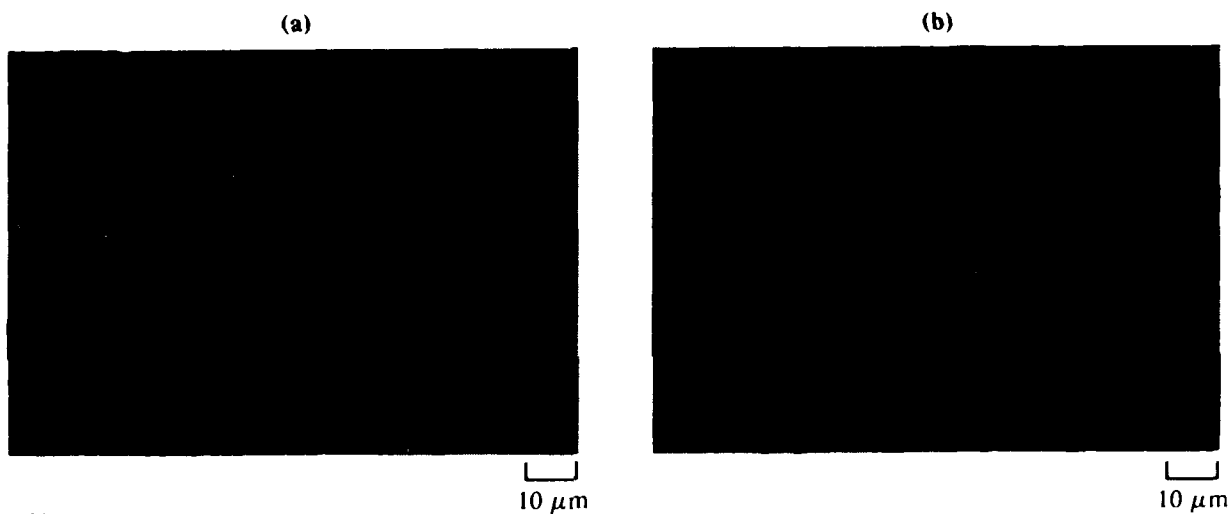


Figure 23. As-cast microstructures of (a) Nb-15W-2La and (b) Nb-30W-2La alloys.

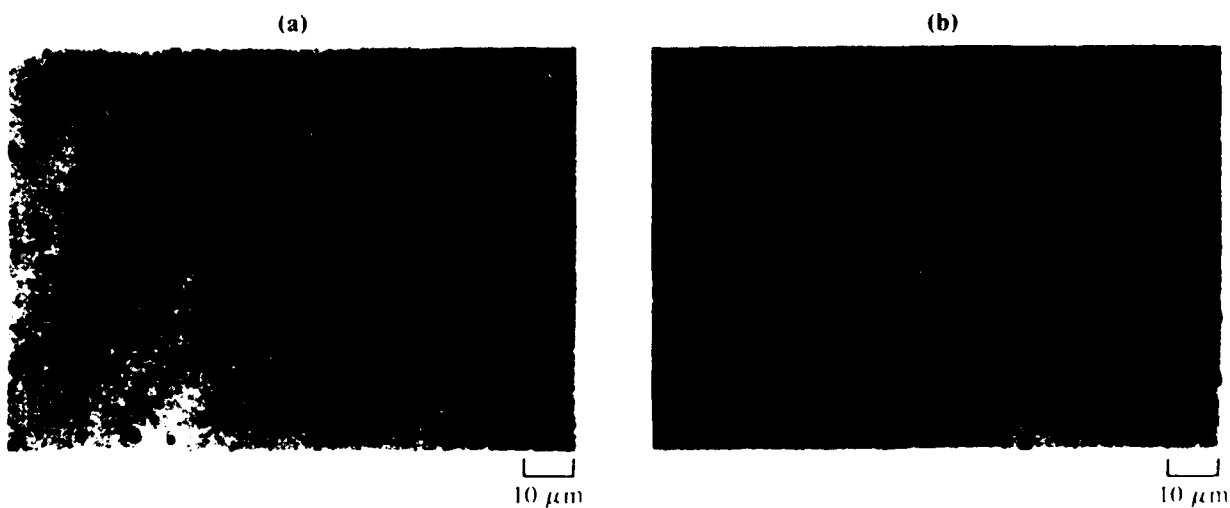
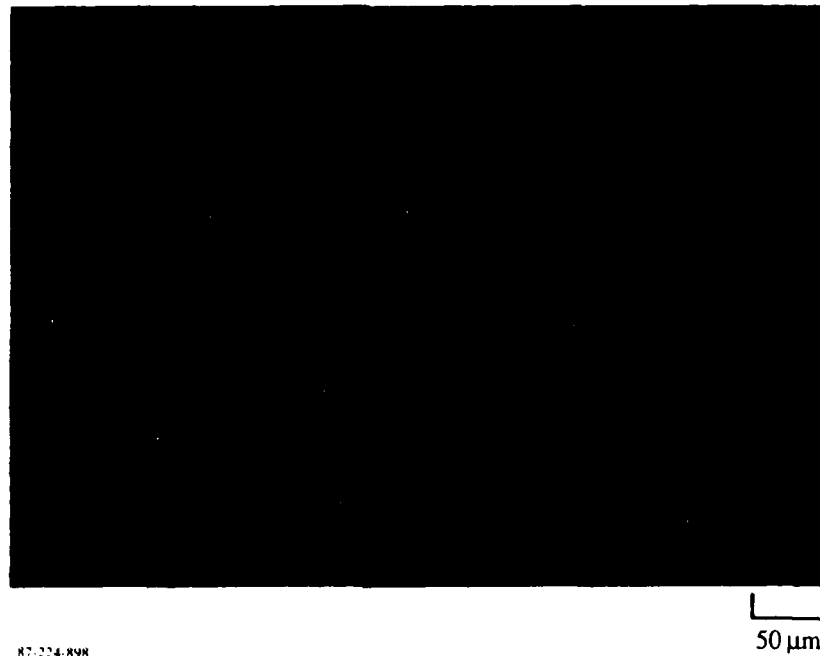
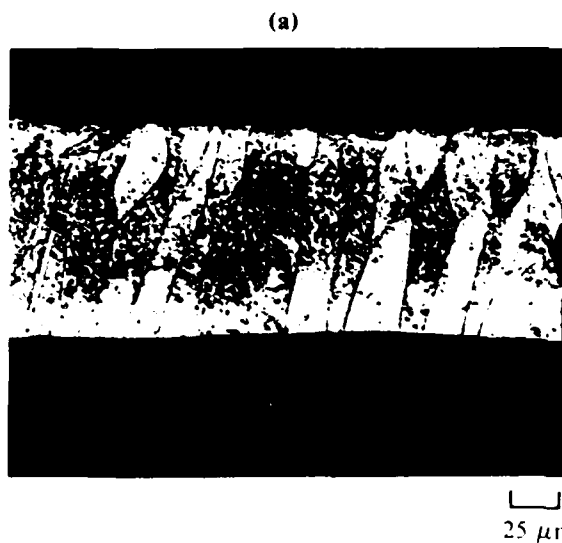


Figure 24. As-cast microstructures of (a) Nb-1Y and (b) Nb-15W-1Y alloys.



K7-224-R98

Figure 25. As-cast microstructure of Nb-0.2C alloy.



K7-224-R98

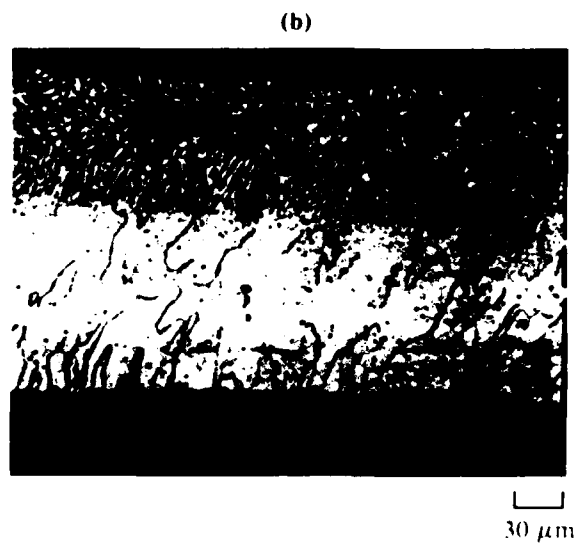


Figure 26. Microstructures of electron beam melted/splat quenched flakes of (a) Nb-21La and (b) Nb-15Hf-1Y alloys.

#### 4. PUBLICATIONS RESULTING FROM THIS CONTRACT

The following publications represent work performed in part under this contract and in part under the McDonnell Douglas Corporation Independent Research and Development program

1. S. M. L. Sastry, "Microstructure Control of Titanium Alloys by Rapid Solidification Processing," presented at the Workshop on Advanced Processing of Intermetallics and Intermetallic Composites, University of California, Santa Barbara, CA, 5-16 January 1987.
2. S. M. L. Sastry, "Effects of Reinforcements on Creep and Fracture Toughness of Titanium Alloys," DARPA Materials Research Council Meeting, La Jolla, CA, 6-10 July 1987.

## 5. LIST OF PERSONNEL

The following MDRL personnel participated in this AFOSR-funded research.

S. M. L. Sastry - Principal Investigator

D. M. Bowden

B. D. London

R. J. Lederich

J. E. O'Neal

## 6. COUPLING ACTIVITIES WITH GROUPS DOING RELATED RESEARCH

1. Presentations on MDRL/AFOSR research on Ti and Nb were made to Mr. Dan Miracle, Mr. Dennis Dimiduk, Mr. Siameck Mazdiazni, and Mr. Bill Kerr (AFWAL/LLM) June 1987.
2. Discussions were held during the TMS/AIME Fall Meeting, Cincinnati, 11-15 October 1987 with Prof. Henry Rack of Clemson University on high-temperature deformation of RST Ti and Nb *in situ* composites, with Bruce MacDonald of National Science Foundation on RST Ti and Nb microstructures, and with Prof. Rama Ankem of University of Maryland on modeling of deformation of *in situ* composites.
3. Discussions were held in January 1987 with Professors J. Perepezko and R. Mehrabian on rapidly solidified microstructures, and with Professors A. G. Evans and B. Budianski on toughening effects of high-modulus reinforcements in Ti alloy matrices.

## 7. REFERENCES

1. S. M. L. Sastry, T. C. Peng, P. J. Meschter, and J. E. O'Neal, "Rapid Solidification Processing of Titanium Alloys," *J. Metals*. 35, 1983, p. 21.
2. S. M. L. Sastry, P. J. Meschter, and J. E. O'Neal, "Structure and Properties of Rapidly Solidified Dispersion-Strengthened Titanium Alloys, Part I: Characterization of Dispersoid Distribution, Structure, and Chemistry," *Metall. Trans.* 15, 1451 (1984).
3. S. M. L. Sastry, T. C. Peng, and L. P. Beckerman, "Structure and Properties of Rapidly Solidified Dispersion-Strengthened Titanium Alloys, Part II: Tensile and Creep Properties," *Metall. Trans.* 15A, 1465 (1984).
4. S. M. L. Sastry, "Dispersion-Strengthened Powder Metallurgy Titanium Alloys," AFWAL TR-83-4092.
5. S. M. L. Sastry, D. M. Bowden, and R. J. Lederich, "Dispersion Strengthening of Ti-Al Alloys by Rapid Solidification Technology," in Titanium Science and Technology, G. Lutjering, U. Zwicker, and W. Bunk, eds. (Deutsche Gesellschaft fur Metallkunde, e.v., FGR, 1985), p. 435.
6. S. M. L. Sastry, T. C. Peng, and J. E. O'Neal, "Design and Development of Advanced Titanium Alloys by Rapid Solidification," in Titanium Science and Technology, G. Lutjering, U. Zwicker, and W. Bunk, eds. (Deutsche Gesellschaft fur Metallkunde, e.v., FGR, 1985), p. 397.
7. T. C. Peng, S. M. L. Sastry, and J. E. O'Neal, "Rapid Solidification Processing of Titanium Alloys," in Titanium Science and Technology, G. Lutjering, U. Zwicker, and W. Bunk, eds. (Deutsche Gesellschaft fur Metallkunde, e.v., FGR, 1985), p. 389.

8. D. M. Bowden and S. M. L. Sastry, "Weldability of Novel Titanium/Rare Earth Alloys Produced by Rapid Solidification Processing," in Titanium Science and Technology, G. Lutjering, U. Zwicker, and W. Bunk, eds. (Deutsche Gesellschaft fur Metallkunde, e.v., FGR, 1985), p. 783.
9. S. M. L. Sastry, R. J. Lederich, and J. E. O'Neal, "Superposition of Solid Solution-, Precipitation-, Grain Size-, Dispersion-Strengthening in Ti-Al-X Alloys," in Titanium Science and Technology, G. Lutjering, U. Zwicker, and W. Bunk, eds. (Deutsche Gesellschaft fur Metallkunde, e.v., FGR, 1985), p. 1811.
10. S. M. L. Sastry, T. C. Peng, and J. E. O'Neal, "Rapid Solidification and Powder Metallurgical Processing of Titanium Alloys," in Modern Developments in Powder Metallurgy, Vol. 16 (Metal Powder Industry Federations, Princeton, New Jersey, 1985), p. 577.
11. J. H. Perepezko and W. J. Boettinger, Proc. Materials Research Society Symposium on Alloy Phase Diagrams, Elsevier-North Holland, pp. 223-229 (1983).
12. T. C. Peng, et al., "Rapid Solidification Processing of Titanium Alloys," Titanium Science and Technology, Deutsche Gesellschaft fur Metallkunde e.v., FRG, pp. 389-395 (1985).
13. Max Hansen and Curt Anderko, Constitution of Binary Alloys, 2nd ed., McGraw-Hill Book Co., New York, p. 260 (1958).
14. Max Hansen and Curt Anderko, Constitution of Binary Alloys, 2nd ed., McGraw-Hill Book Co., New York, p. 383 (1958).
15. B. Aronson, et al. Borides, Silicides and Phosphides, John Wiley, New York, pp. 47-56 (1965).
16. H. R. Ogden, et al., "Structure and Properties of Ti-C Alloys," Trans. TMS-AIME, Vol. 203, No. 1, pp. 73-80 (January 1955).

END  
DATE  
FILMED  
DTIC  
4/88